

Article

# Beyond Contrail Avoidance: Efficacy of Flight Altitude Changes to Minimise Contrail Climate Forcing

Roger Teoh<sup>1</sup>, Ulrich Schumann<sup>2</sup>  and Marc E. J. Stettler<sup>1,\*</sup>

<sup>1</sup> Centre for Transport Studies, Department of Civil and Environmental Engineering, Imperial College London, London SW7 2AZ, UK; roger.teoh15@imperial.ac.uk

<sup>2</sup> Institute of Atmospheric Physics, Deutsches Zentrum für Luft- und Raumfahrt, 82234 Oberpfaffenhofen, Germany; Ulrich.Schumann@dlr.de

\* Correspondence: m.stettler@imperial.ac.uk

Received: 30 July 2020; Accepted: 18 August 2020; Published: 21 August 2020



**Abstract:** Contrail cirrus introduce a short-lived but significant climate forcing that could be mitigated by small changes in aircraft cruising altitudes. This paper extends a recent study to evaluate the efficacy of several vertical flight diversion strategies to mitigate contrail climate forcing, and estimates impacts to air traffic management (ATM). We use six one-week periods of flight track data in the airspace above Japan (between May 2012 and March 2013), and simulate contrails using the contrail cirrus prediction model (CoCiP). Previous studies have predominantly optimised a diversion of every contrail-forming flight to minimise its formation or radiative forcing. However, our results show that these strategies produce a suboptimal outcome because most contrails have a short lifetime, and some have a cooling effect. Instead, a strategy that reroutes 15.3% of flights to avoid long-lived warming contrails, while allowing for cooling contrails, reduces the contrail energy forcing ( $EF_{\text{contrail}}$ ) by 105% [91.8, 125%] with a total fuel penalty of 0.70% [0.66, 0.73%]. A minimum  $EF_{\text{total}}$  strategy (contrails +  $\text{CO}_2$ ), diverting 20.1% of flights, reduces the  $EF_{\text{contrail}}$  by the same magnitude but also reduces the total fuel consumption by 0.40% [0.31, 0.47%]. For the diversion strategies explored, between 9% and 14% of diversions lead to a loss of separation standards between flights, demonstrating a modest scale of ATM impacts. These results show that small changes in flight altitudes are an opportunity for aviation to significantly and rapidly reduce its effect on the climate.

**Keywords:** aviation; contrail cirrus; climate forcing; mitigation; air traffic management

## 1. Introduction

Contrails form behind an aircraft when the atmospheric conditions are favourable (high humidity and low temperatures) [1,2]. Black carbon (BC) particles and water vapour emitted from the exhaust of aircraft engines play a key role in this process [3,4]: hot aircraft exhaust mixes with cool ambient air causing an increase in relative humidity; liquid water droplets form on the surface of BC particles when the humidity in this mixture exceeds liquid saturation and these droplets then freeze into ice crystals. The BC number emissions index ( $EI_n$  in  $\text{kg}^{-1}$ ) therefore determines the initial number of contrail ice particles, which then influences various contrail characteristics including the ice particle size, lifetime, optical and radiative properties [5,6].

Most contrails have lifetimes of less than 10 min [7,8]. However, contrails can persist when the relative humidity in the ambient air exceeds 100% with respect to ice (RH<sub>i</sub>) and develop into contrail cirrus, a mixture of line-shaped and irregularly shaped contrails and other cirrus clouds. These contrails can have lifetimes of up to a day [9–11] and may cover a large fraction of the sky area

in regions with high air traffic density (ATD) [12–14]. During daytime, contrails scatter part of the incoming shortwave (SW) solar radiation back to space causing a cooling of the Earth–atmosphere system below the contrails, and maximum cooling is attained when the solar zenith angle is between 40° and 60° [15]. At all times, however, contrails trap part of the terrestrial radiation, reducing the outgoing longwave (LW) infrared radiation and induce a warming greenhouse effect [16,17].

Several metrics have been used to quantify the contrail climate forcing. The radiative forcing (RF, in units of  $\text{W m}^{-2}$ ) quantifies the change in radiative energy flux by contrails from a fleet of aircraft over a given spatiotemporal domain; while the local contrail RF (RF'), defined as the change in energy flux per contrail area, describes the climate forcing of individual contrail segments [15]. The ratio of SW/LW RF depends strongly on the microphysical optical properties of contrail ice particles and on factors affecting radiation transfer in the Earth-atmosphere system [17]. There is scientific consensus that the warming effect dominates [8]. Previous studies found a wide range of SW/LW ratios, varying between 0.2 and 0.8 [18]. Some early global models assumed spherical ice crystals and computed SW/LW ratios close to 0.2 [12,19]. More recent studies found larger ratios of between 0.4 and 0.6 [20,21], which implies a stronger potential for contrails to cool the Earth surface during daytime. On average, the global annual mean net RF of contrail cirrus ( $\approx 0.01$  to  $0.09 \text{ W m}^{-2}$ ) [8,12,18,22,23] has been estimated to be comparable to the RF from aviation's cumulative  $\text{CO}_2$  emissions ( $\approx 0.015$  to  $0.04 \text{ W m}^{-2}$ ) [22]. As air traffic is not uniform across the world, the contrail net RF can be greater than  $1 \text{ W m}^{-2}$  in regions with high ATD [24,25], and scaling down further, the RF' can exceed  $\pm 60 \text{ W m}^{-2}$  for optically thick individual contrail segments [9,26].

An alternative metric, the contrail energy forcing ( $\text{EF}_{\text{contrail}}$ , in units of J), which can be normalised with the flight distance or contrail length ( $\text{J m}^{-1}$ ), is calculated as the contrail RF' multiplied by its width and integrated over its length and lifetime [23,27]. By capturing the evolving contrail dimensions and RF', the  $\text{EF}_{\text{contrail}}$  quantifies the cumulative contrail climate forcing from individual flights, rather than the RF at an instantaneous point in time. The mean  $\text{EF}_{\text{contrail}}$  per flight distance amounts to about  $0.4$  to  $0.7 \times 10^8 \text{ J m}^{-1}$ , and contrails with the largest positive  $\text{EF}_{\text{contrail}}$  are generally formed late in the afternoon [28].

Various mitigation solutions have been proposed to reduce contrail formation and its climate forcing (RF or EF). For example, the use of cleaner-burning engines and alternative biofuels, which reduces the aircraft BC  $\text{EI}_n$  by one order of magnitude [29–32], can reduce the contrail lifetime, light scattering efficiency, optical depth ( $\tau$ ) and RF [2,33]. However, cleaner-burning engines can only be adopted at scale over the long-term because aircraft typically have long lifecycles ( $>20$  years) [34,35], while biofuels, which currently only account for 0.01% of global jet fuel consumption [36,37], can facilitate contrail formation and reduce a contrail's efficacy in reflecting incoming solar radiation [38,39].

Flight diversion strategies that reroute air traffic around ice-supersaturated regions appear to be the most feasible contrail mitigation solution that could be implemented in the near-term. ISSRs are commonly found in the upper troposphere at altitudes of between 8 and 13 km, and have average horizontal and vertical extensions of  $150 \pm 250 \text{ km}$  and  $0.7 \pm 0.1 \text{ km}$ , respectively [8,40–42]. A range of operational strategies have been explored, including lateral/horizontal diversions [11,43], altitude changes [23,28,44–46], and a combination of lateral and vertical diversions [47,48]. However, a strategy that diverts all contrail-forming flights to minimise its formation, predominantly advocated by earlier studies [23,45–49], might produce a suboptimal outcome because: (i) some contrails are short-lived and/or can have a cooling effect; (ii) the increase in fuel consumption and long-lived  $\text{CO}_2$  emissions could outweigh the climate benefits of contrail mitigation; and (iii) it can be highly disruptive to air traffic management (ATM) [50]. In our previous study [28], we addressed issues (i) and (ii) and showed that only 2% of all flights in the Japanese airspace were responsible for 80% of the total  $\text{EF}_{\text{contrail}}$ , and diverting up to 1.7% of flights by  $\pm 2000$  feet could reduce the  $\text{EF}_{\text{contrail}}$  by up to 59% [52, 66%] at a 95% confidence interval (CI), with a 0.014% [0.010, 0.017%] increase in total fuel burn and  $\text{CO}_2$  emissions. On top of diverting flights with the largest  $\text{EF}_{\text{contrail}}$ , flights can also be rerouted [51] or rescheduled [52,53] to form cooling contrails and offset the warming effects of  $\text{CO}_2$  emissions. One study [19] used a model

with a low ratio of SW/LW RF and found that rescheduling night flights to fly in daytime is ineffective at reducing the contrail cirrus RF [19], but that result may differ for a larger SW/LW ratio. Hence, the mitigation potential of a strategy that maximises the cooling effect of contrails (negative  $EF_{\text{contrail}}$ ) remains unexplored. Furthermore, although a small-scale diversion may limit the potential impacts on ATM, the number of ATM conflicts where flights violate the minimum separation standards has not yet been quantified.

Given these research gaps, this paper therefore aims to: (i) evaluate the efficacy of alternative vertical flight diversion strategies beyond contrail avoidance; and (ii) quantify the potential impacts of selected diversion strategies to ATM, in terms of the loss of separation (LOS) standards between flights. Five strategies are considered, where the trajectories of all flights are selected to minimise the: (i) contrail length; (ii) mean contrail RF; (iii)  $EF_{\text{contrail}}$ ; (iv)  $EF_{\text{contrail}}$  with an additional constraint that flights are only diverted if they do not incur a fuel penalty; and (v)  $EF_{\text{total}}$  (including the EF of both contrails and  $\text{CO}_2$ ). In our previous study [28], the diversion of flights was constrained to only those with the largest  $EF_{\text{contrail}}$ , while the present study allows for any number of flights to be diverted and for flights to form cooling contrails (with a negative contrail RF' and/or EF).

## 2. Data and Methodology

Contrails that are formed by individual flights in the airspace above Japan were simulated to assess the efficacy of a vertical flight diversion strategy (reroutes based on altitude changes) and its impact on ATM. Several datasets and models were used to achieve these objectives: an aircraft activity dataset, an estimate of aircraft fuel consumption and emissions, meteorological data, and a contrail model. A detailed description of these datasets and models was previously published in Teoh et al. [28]. Here, we provide a summary of these datasets and models, and highlight any changes that were made to the methods for this paper.

### 2.1. Aircraft Activity and Emissions

The 2012 CARATS Open Data provides aircraft trajectory data in Japan's four main Area Control Centres (ACC): Tokyo, Fukuoka, Sapporo and Naha ACC. Six one-week periods of air traffic data were provided bimonthly between May 2012 and March 2013, capturing 149,117 distinct flights. The data for each flight contains a censored flight ID, an International Civil Aviation Organization (ICAO) aircraft type designator, and their 3D position is tracked by en-route radars at 0.1 Hz. Aircraft-engine assignments were provided by Stettler et al. [54], and the Base of Aircraft Data (BADA 3) was used to estimate the thrust ( $F$ ) and fuel mass flow rate ( $\dot{m}_f$ ) for each waypoint and the total fuel consumption (TFC) of each flight [55].  $F$  and  $\dot{m}_f$  were subsequently used to estimate several engine parameters, including: (i) the overall propulsion efficiency, which can influence the onset of contrail formation [56]; as well as the (ii) engine thrust settings ( $F/F_{00,\text{max}}$ , where  $F_{00,\text{max}}$  is the maximum rated thrust at sea level and zero speed); and (iii) the ratio of the turbine inlet to compressor inlet temperatures ( $T_4/T_2$ ). Parameters (ii) and (iii) were required to estimate the aircraft BC  $EI_n$ .

The aircraft BC  $EI_n$ , which varies with aircraft type and engine power, was estimated using the Fractal Aggregates (FA) model [28,57]. The FA model estimates the aircraft BC  $EI_n$  from the BC mass emissions index, particle size distribution and morphology because measurements and models for these parameters are more readily available [28].

### 2.2. Contrail Simulation and Uncertainty

The contrail cirrus prediction model (CoCiP) was used to simulate the properties of individual contrail segments throughout its lifecycle [5]. A contrail segment is formed when two consecutive waypoints of a flight satisfy the Schmidt–Appleman criterion for contrail formation [3]. Further details on CoCiP can be found in the literature [5,15], and the modelled contrail outputs have previously been validated with in situ measurements and satellite observations [5,9,18,58–61].

CoCiP requires inputs of air traffic data (CARATS Open Data), estimates of aircraft BC  $EI_n$  (FA model) and meteorology. We used reanalysis meteorological data from the European Centre for Medium-Range Weather Forecasts (ECMWF), the ERA5 ten-member ensemble (EDA) [62]: it contains the ten-member ensemble means and standard deviations of the required parameters (specific humidity, ambient temperature, U- and V- component of wind, vertical velocity, geopotential and specific cloud ice water content) at a sequence of 37 pressure levels and a spatiotemporal resolution of  $0.5^\circ \times 0.5^\circ$  and 3 h, respectively.

Uncertainties in meteorology (estimated from the ERA5 EDA and assumed to be normally distributed) [63] influence the estimated TFC and aircraft BC  $EI_n$ . The input parameters of the FA model were also subject to uncertainties, and propagating them to the BC  $EI_n$  results in an uncertainty of  $[-70, +200\%]$  at 95% CI that is lognormally distributed [28]. We then used a Monte Carlo 100-member ensemble to propagate the uncertainties arising from meteorology and aircraft BC  $EI_n$  to account for uncertainties in the modelled contrail outputs. While Teoh et al. [28] previously assumed that the uncertainties between meteorological parameters were independent, we defined the uncertainties of specific humidity and ambient temperature to be correlated because the saturation vapour pressure decreases with ambient temperature. The seed used to generate the random uncertainty factors for each input variable (BC  $EI_n$  and meteorology) in the Monte Carlo simulation were also fixed to ensure that the conditions were consistent among different strategies and that model outputs were reproducible.

The contrail uncertainties do not account for model uncertainties [5]. For example, the model assumes radiation transfer in a plane-parallel atmosphere, but 3D radiation transfer may be important for narrow contrails [64–66]. Uncertainties arising from different contrail models, the radiative transfer scheme, efficacy of global surface temperature response and other climate parameters to RF [67], and the question of validating the difference in contrail effects that can be attributed to flight reroutes have been identified earlier [28], and remain to be investigated beyond this study.

### 2.3. Climate Forcing of Contrails and $CO_2$

The simulated contrail properties (including ice particle radius and optical thickness), meteorology and radiation (ERA5 EDA) were used as inputs to a parameterised algebraic model described in Schumann et al. [15] to estimate the RF' for each contrail segment, which was then used to estimate the  $EF_{\text{contrail}}$ ,

$$EF_{\text{contrail}} [J] = \int_0^T RF'(t) \times L(t) \times W(t) dt \quad (1)$$

where  $L$  and  $W$  are the contrail length and width at time  $t$ , and  $T$  is the lifetime of the contrail segment. Equation (1) captures the evolving contrail dimensions and RF' over its lifetime and highlights contrails that persist and spread, as these lead to a greater imbalance in the Earth's radiation budget. The total  $EF_{\text{contrail}}$  is the sum of the EF from all contrail segments and all flights.

Diversion strategies that mitigate the short-lived contrail climate forcing can lead to unintended consequences of increasing the  $CO_2$  emissions that could remain in the atmosphere for centuries [68]. Therefore, it is important to compare the climate forcing of contrails and  $CO_2$  with a metric that accounts for differences in their lifetime. While the EF concept is not generally used for gaseous pollutants such as  $CO_2$ , it can be approximated by integrating the  $CO_2$  RF over a given time-horizon (20, 100 or 1000 years) and multiplying it with the Earth's surface area because it is well-mixed in the atmosphere.

$$EF_{CO_2} [J] = \int_0^{TH} RF_{CO_2} dt \times S_{\text{Earth}} = [AGWP_{CO_2, TH} \times (365 \times 24 \times 60^2)] \times TFC \times EI_{CO_2} \times S_{\text{Earth}} \quad (2)$$

where  $AGWP_{CO_2, TH}$  is the  $CO_2$  absolute global warming potential over a selected time-horizon (TH) [68],  $EI_{CO_2}$  is the  $CO_2$  emissions index ( $3.16 \text{ kg kg}^{-1}$ ) [69] and  $S_{\text{Earth}}$  is the surface area of Earth ( $5.101 \times 10^{14} \text{ m}^2$ ) [70]. The number of seconds per year occurs in Equation (2) because the  $AGWP_{CO_2}$

commonly refers to annual emissions and is given in units of  $\text{y W m}^{-2} \text{ kg}^{-1}$ . We used a 100-year TH in evaluating  $\text{CO}_2$  emissions,  $\text{AGWP}_{\text{CO}_2, 100} = 92.5 [68, 117] \times 10^{-15} \text{ year Wm}^{-2} \text{ kg}^{-1}$ , 95% CI [68], consistent with the Kyoto Protocol, and where necessary, evaluate the sensitivity of  $\text{EF}_{\text{CO}_2}$  to TH by using a 1000-year ( $\text{AGWP}_{\text{CO}_2, 1000} = 548 [380, 716] \times 10^{-15} \text{ year Wm}^{-2} \text{ kg}^{-1}$ ) TH for the  $\text{AGWP}_{\text{CO}_2}$  [68].

#### 2.4. Contrail Mitigation

Two alternative trajectories were generated for each flight in addition to the original trajectory: cruising altitudes were uniformly modified by  $\pm 2000$  feet relative to the original trajectory (baseline scenario). The higher trajectory (+2000 feet) is only available when its waypoints do not exceed the altitude service ceiling for specific aircraft types. We computed the TFC for the new trajectories using BADA 3, accounting for the change in fuel consumption when climbing/descending to the new cruising altitude and for differences in the ambient meteorological conditions (wind and temperature). The contrail properties and climate forcing were then computed with CoCiP for the three trajectories. The accuracy of the changes in estimated TFC (between the original and alternative trajectories) were subjected to known limitations of BADA 3 in approximating the dependencies of fuel consumption on Mach number, lift coefficient and Reynolds number for variable aircraft mass, flight level and ambient temperature [71]. Possibly improved methods, which account for these effects, are presently under development [72] or have restricted access (BADA 4) [73]. For each Monte Carlo simulation, uncertainties in the meteorology and the BC  $\text{EI}_n$  for specific flights were specified consistently between the original and alternative trajectories (Section 2.2).

Five distinct strategies were considered, where the trajectories of all flights were selected to minimise one of the five objective functions: (i) initial contrail length; (ii) mean contrail  $\text{RF}'$ ; (iii)  $\text{EF}_{\text{contrail}}$ ; (iv)  $\text{EF}_{\text{contrail}}$  with an additional constraint where only flights that do not incur a fuel penalty were diverted; and (v)  $\text{EF}_{\text{total}}$  ( $\text{EF}_{\text{contrail}} + \text{EF}_{\text{CO}_2}$  with a 100-year TH). We reiterate that our previous study [28] constrained the diversion of flights to only those with the largest  $\text{EF}_{\text{contrail}}$ , while this study expands the search space by allowing for any number of flights to be diverted and flights can form cooling contrails (with a negative contrail  $\text{RF}'$  and/or  $\text{EF}$ ). To evaluate the efficacy of each strategy, the percentage of flights that require diversion, as well as the change in TFC, contrail properties and climate forcing were quantified at a 95% CI.

#### 2.5. Loss of Separation

Flight diversion strategies were expected to create ATM disruptions by increasing complexity, airspace congestion, and the number of incidences where aircraft pairs experience a loss of separation (LOS) [50,74]. Hence, ATM considerations could limit the scale and effectiveness of any proposed diversion strategy. However, most studies have not accounted for these unintended consequences, apart from Grewe et al. [48] and Rosenow et al. [49] which both specified the minimum separation standards as a constraint in optimising flight trajectories.

Airspace that is covered by radar, such as the Tokyo, Fukuoka, Sapporo and Naha ACC, typically operate with the Reduced Vertical Separation Minimum standard, where flights adhere to a separation minima of 1000 feet vertically and 5 nautical miles (NM) laterally [75,76]. A LOS event was recorded when distinct aircraft pairs violate the separation minima standards. Here, we quantify the number of conflicts/LOS that were introduced from three diversion strategies: (i) the small-scale diversion proposed by Teoh et al. [28], where 1.7% of flights with the largest  $\text{EF}_{\text{contrail}}$  are diverted; and (ii) the minimum  $\text{EF}_{\text{contrail}}$  strategy, a larger scale diversion where all flights are diverted to the altitude that minimises their  $\text{EF}_{\text{contrail}}$ ; and (iii) the minimum  $\text{EF}_{\text{contrail}}$  strategy with the constraint that only flights that did not incur a fuel penalty were diverted. Strategies (ii) and (iii) were previously described in Section 2.4.

We interpolated the position of each flight every minute, flag waypoints with a LOS, and aggregate the number of aircraft pairs and flights that were in conflict on an hourly basis. Aircraft pairs that have successive waypoints with a LOS were recorded only once at the time when their separation is at a

minimum. We did not check for a LOS between flights when their altitude is below 20,000 feet because persistent contrails do not generally form below these altitudes and the separation standards in these phases of flight can be smaller relative to cruise conditions [75]. The full Monte Carlo simulation was not run because of the large computational requirements (one simulation run to check for ATM violations takes approximately 24 h). For the three diversion strategies, we used the set of optimal flight trajectories that were provided by the first run of their Monte Carlo simulation.

### 3. Results and Discussion

#### 3.1. Efficacy of Flight Altitude Changes

Table 1 shows the aggregated contrail properties and climate forcing ( $RF'$  and  $EF_{\text{contrail}}$ ), total fuel consumption,  $EF_{\text{CO}_2}$  and  $EF_{\text{total}}$  for all flights in the CARATS Open Data in the baseline scenario. While the datasets and models used are the same as in our previous study [28], results from the baseline scenario differs slightly: the percentage of flights forming contrails increased from 17.8% [17.2, 18.4%] to 21.4% [21.1, 21.9%]; the mean contrail segment age increased from 3.24 [3.09, 3.36] h to 4.37 [4.13, 4.63] h (+35.0%); and the aggregated  $EF_{\text{contrail}}$  increased from 5.38 [3.85, 6.66] to 5.75 [4.12, 8.45]  $\times 10^{18}$  J (+6.93%). This is because we now assume that the uncertainties of ambient temperature and specific humidity are correlated (Section 2.2), which leads to a smaller variance in the RHi between Monte Carlo simulations.

The percentage differences in these aggregated metrics from the various vertical flight diversion strategies (see Section 2.4) are shown in Table 1 and Figure 1. In general, the choice of strategy leads to different efficacies in mitigating the contrail climate forcing: minimising the initial contrail length (contrail avoidance) or the  $RF'$ , commonly adopted by previous studies [11,44–49], reduces the aggregated  $EF_{\text{contrail}}$  by 70.8% [66.0, 75.3%] and 74.6% [65.4, 89.6%], respectively. However, a strategy that minimises the cumulative contrail climate forcing over contrail lifetimes (minimum  $EF_{\text{contrail}}$ ) achieves a larger reduction in the  $EF_{\text{contrail}}$ , by 105% [91.8, 125%]. For these three strategies (minimum contrail length,  $RF'$  and  $EF_{\text{contrail}}$ ), the TFC increases slightly by up to 0.70% [0.66, 0.73%]. The two remaining strategies minimise either the  $EF_{\text{contrail}}$  or the  $EF_{\text{total}}$  (accounting for the EF of contrails and  $\text{CO}_2$ ) under an additional constraint that flights are only diverted if they do not incur a fuel penalty: the first variant reduces both the  $EF_{\text{contrail}}$  by 52.1% [42.5, 60.8%] and TFC by 0.86% [0.84, 0.88%]; while the second variant reduces the  $EF_{\text{contrail}}$  and TFC by 105% [91.8, 125%] and 0.40% [0.31, 0.47%], respectively.

For all five strategies, the percentage of flights that are selected for diversion (ranging between 7.6% and 20.1%) is significantly larger than the small-scale diversion strategy proposed in our earlier study [28] (up to 1.7% of all flights). This is because the earlier study [28] investigated a strategy of diverting the 2% of flights that contribute to 80% of the total  $EF_{\text{contrail}}$ , while the search space in this study is larger and considers alternative trajectories for all flights to minimise the selected objective function. We discuss the results for each strategy in detail in the subsections below.

**Table 1.** Aggregated contrail properties (initial contrail length and mean contrail segment age) and climate forcing (RF' and EF<sub>contrail</sub>), total fuel consumption, EF<sub>CO<sub>2</sub></sub> and EF<sub>total</sub> for the baseline scenario (top); as well as the percentage of flights diverted and percentage difference of these quantities for the five strategies relative to the baseline scenario (bottom). The EF<sub>CO<sub>2</sub></sub> and EF<sub>total</sub> presented in this table are calculated based on a 100-year time-horizon (TH) for the CO<sub>2</sub> AGWP, and the 95% CI is provided in the square brackets.

		Initial Contrail Length (10 <sup>9</sup> m)	Mean Contrail Segment Age (h)	Mean Contrail RF' (W m <sup>-2</sup> )	EF <sub>contrail</sub> (10 <sup>18</sup> J)	Total Fuel Consumption, TFC <sup>a</sup> (10 <sup>8</sup> kg)	EF <sub>CO<sub>2</sub></sub> <sup>a,b</sup> (10 <sup>18</sup> J)	EF <sub>total</sub> <sup>b</sup> (10 <sup>18</sup> J; Contrails + CO <sub>2</sub> )
<b>Baseline Scenario</b>		6.933 [6.813, 7.312]	4.373 [4.126, 4.629]	1.420 [0.940, 2.200]	5.753 [4.119, 8.449]	2.90716 [2.90710, 2.90721]	3.4277 [1.7187, 5.0480]	9.037 [6.468, 12.280]
<b>Percentage Difference Relative to the Baseline Scenario</b>								
	% of Flights Diverted	Initial Contrail Length	Mean Contrail Segment Age	Mean Contrail RF'	EF <sub>contrail</sub>	Total Fuel Consumption, TFC	EF <sub>CO<sub>2</sub></sub> <sup>b</sup>	EF <sub>total</sub> <sup>b</sup>
<b>Min. Contrail Length</b>	12.9% [12.8, 13.2%]	-66.6% [-67.0, -65.8%]	-3.61% [-5.54, -0.59%]	-29.2% [-63.2, -12.4%]	-70.8% [-75.3, -66.0%]	+0.57% [+0.55, +0.59%]	+0.24% [+0.23, +0.24%]	-45.0% [-55.9, -38.6%]
<b>Min. Contrail RF'</b>	15.0% [14.7, 15.3%]	-17.3% [-20.3, -13.5%]	-9.05% [-10.6, -7.21%]	-186% [-282, -122%]	-74.6% [-89.6, -65.4%]	+0.69% [+0.66, +0.72%]	+0.28% [+0.27, +0.30%]	-47.2% [-59.0, -40.5%]
<b>Min. EF<sub>contrail</sub></b>	15.3% [15.0, 15.7%]	-23.1% [-27.6, -17.4%]	-13.9% [-16.4, -11.4%]	-185% [-279, -121%]	-105% [-125, -91.8%]	+0.70% [+0.66, 0.73%]	+0.29% [+0.27, +0.30%]	-66.7% [-83.7, -57.2%]
<b>Min. EF<sub>contrail</sub> (No Fuel Penalty)</b>	7.63% [7.47, 7.81%]	-8.64% [-10.7, -6.66%]	-4.90% [-6.06, -4.20%]	-75.7% [-119, -46.1%]	-52.1% [-60.8, -42.5%]	-0.86% [-0.88, -0.84%]	-0.36% [+0.27, +0.30%]	-32.4% [-41.7, -27.4%]
<b>Min. EF<sub>total</sub> (CO<sub>2</sub> + Contrail)</b>	20.1% [19.9, 20.3%]	-23.2% [-27.7, -17.4%]	-13.7% [-16.3, -11.3%]	-183% [-275, -120%]	-105% [-125, -91.8%]	-0.40% [-0.47, -0.31%]	-0.17% [-0.20, -0.13%]	-66.8% [-83.9, -57.4%]

<sup>a</sup> shown to 5–6 significant figures to allow identification of differences in values. <sup>b</sup> CO<sub>2</sub> EF is calculated with a TH of 100-years (Section 2.3).

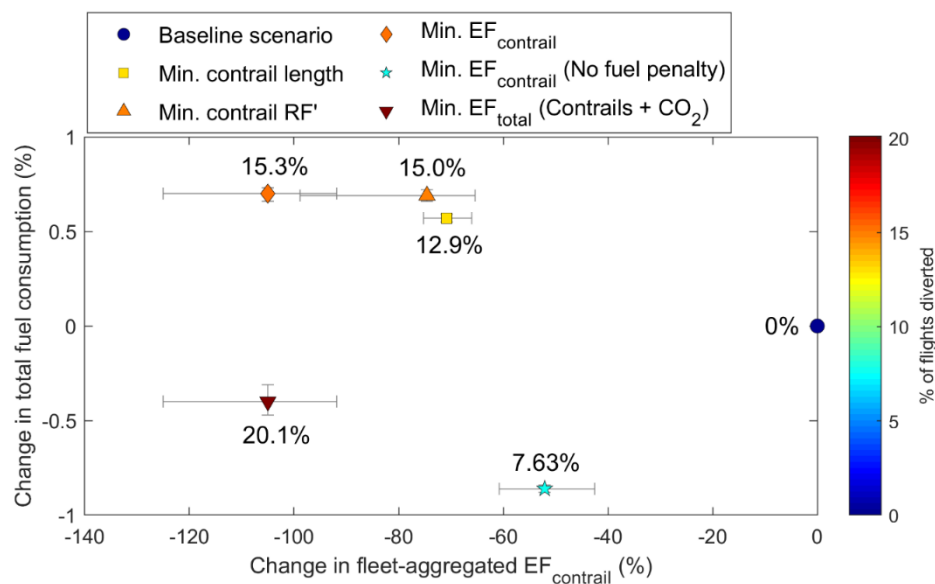


**Figure 1.** Percentage change in the aggregated contrail energy forcing ( $EF_{\text{contrail}}$ ) and total fuel consumption (TFC; for all flights in the dataset) for vertical flight diversion strategies with five different objective functions relative to the baseline scenario. The strategies include selecting the flight trajectories with a minimum: (i) contrail length; (ii) local contrail radiative forcing ( $RF'$ ); (iii)  $EF_{\text{contrail}}$ ; (iv)  $EF_{\text{contrail}}$  with an additional constraint where flights with no fuel penalty are diverted; and (v)  $EF_{\text{total}}$ , including the  $EF$  of contrails and  $CO_2$ . The percentage of flights diverted is shown in the symbol colour. Error bars denote the 95% CI.

### 3.1.1. Contrail Avoidance

The contrail avoidance strategy requires the diversion of 12.9% [12.8, 13.2%] of all flights to reduce the initial contrail length, i.e., the total length of flight distance forming contrails, by 66.6% [65.8, 67.0%] with an increase in TFC of 0.57% [0.55, 0.59%] (Table 1). However, reductions in the mean contrail age ( $-3.61\%$  [ $-5.54, -0.59\%$ ]),  $RF'$  ( $-29.2\%$  [ $-63.2, -12.4\%$ ]),  $EF_{\text{contrail}}$  ( $-70.8\%$  [ $-75.3, -66.0\%$ ]) and  $EF_{\text{total}}$  ( $-45.0\%$  [ $-59.0, -40.5\%$ ]) that can be achieved from this strategy are lower than the other strategies explored in Table 1. We note that a pure contrail avoidance strategy can lead to unintended consequences: 16.0% [14.8, 17.2%] of the diverted flights successfully reduced their proportion of flight distance forming contrails, but the contrail age and/or  $EF$  from their selected trajectory are larger than the original trajectory. This includes cases where flights were originally forming cooling contrails (with a negative  $EF_{\text{contrail}}$ ), but a diversion prevents any contrails from forming. Hence, the simple contrail avoidance strategy cannot be recommended because those that are present during the day can have a cooling effect, and the trajectory that produces a shorter contrail length could have a longer lifetime and larger  $EF_{\text{contrail}}$ .

### 3.1.2. Minimum Contrail $RF'$

The strategy to minimise the contrail  $RF'$  leads to a reduction in the mean contrail  $RF'$  ( $-186\%$  [ $-282, -122\%$ ]),  $EF_{\text{contrail}}$  (74.6% [65.4, 89.6%]) and  $EF_{\text{total}}$  (47.2% [40.5, 59.0%]) at the expense of a 0.69% [0.66, 0.72%] increase in TFC. It diverts slightly more flights (15.0% [14.7, 15.3%]) than the contrail avoidance strategy, but further gains in reducing  $EF_{\text{contrail}}$  and  $EF_{\text{total}}$  are marginal. The additional gain is small because the contrail  $RF'$  is minimised regardless of changes in the contrail age and its cumulative climate forcing: contrails become optically thinner (lower  $\tau$ ) as they spread over time [21,27], implying that longer-lived contrails can have a smaller mean contrail  $RF'$  because it is proportional to  $\tau$  [15]. This could lead to the strategy favouring a trajectory that produces long-lived contrails with a weaker  $RF'$ : 35.0% [34.1, 36.1%] of the diverted flights have a larger contrail age than their original trajectory, and 20.7% [20.1, 21.2%] of them have a larger  $EF_{\text{contrail}}$ . Although flights can also be diverted

to a trajectory with a large negative contrail  $RF'$ , their overall cooling effect (in terms of the negative  $EF_{\text{contrail}}$ ) can be insignificant if the contrail lifetime is short and/or small coverage area. Similarly, it might not be necessary to divert flights with a large positive contrail  $RF'$  if they are short-lived and have negligible radiative significance.

### 3.1.3. Minimum $EF_{\text{contrail}}$

The strategy minimising the  $EF_{\text{contrail}}$  diverts 15.3% [15.0, 15.7%] of flights, a proportion that is similar to the minimum contrail  $RF'$  strategy, but achieves a larger reduction in  $EF_{\text{contrail}}$  (105% [91.8, 125%]) and  $EF_{\text{total}}$  (66.7% [57.2, 83.7%]) with a small increase in TFC (0.70% [0.66, 0.73%]). There is a 65% probability that this strategy changes the sign of the total contrail climate forcing from warming to cooling (negative  $EF_{\text{contrail}}$ ). The cooling slightly offsets the warming effects of long-lived  $CO_2$  emissions.

For the six one-week periods of air traffic data available, flights that produce the largest  $EF_{\text{contrail}}$  generally occur between 10:00 and 22:00 Japan local time (Figure 2a). The time of day when the largest  $EF_{\text{contrails}}$  are formed depends on the seasonality [28]: during the summer with longer daylight hours, flights with a large  $EF_{\text{contrail}}$  are typically formed after 15:00 local time; while flights that are flown before noon can also produce the largest  $EF_{\text{contrail}}$  in winter because of the shorter daylight hours. Although persistent contrails forming at these times can induce a cooling effect initially, the spreading contrail (coverage area can grow by one order of magnitude after a few hours [12,77,78]) and positive  $RF'$  during the night both enhance its warming effect [28]. Figure 2b shows that the minimum  $EF_{\text{contrail}}$  strategy favours: (i) the diversion of flights that produces long-lived contrails with lifetimes longer than 8 h, where fewer data points with a large  $EF_{\text{contrail}}$  are observed at all times; and (ii) the formation of cooling contrails from midnight to around 15:00 local time, as shown by an increased number of data points with a larger negative  $EF_{\text{contrail}}$  at these times. While the diversion of flights to form contrails during the night (that induce a positive  $EF_{\text{contrail}}$  initially) seems counterintuitive in mitigating the contrail climate forcing, their cooling effects are maximised after dawn because these persistent contrails have grown to a large coverage area with a negative  $RF'$ . The potential disruptions to ATM that is caused by these diversions would likely be at a minimum because the ATD is low during those times, as will be evaluated in Section 3.2.

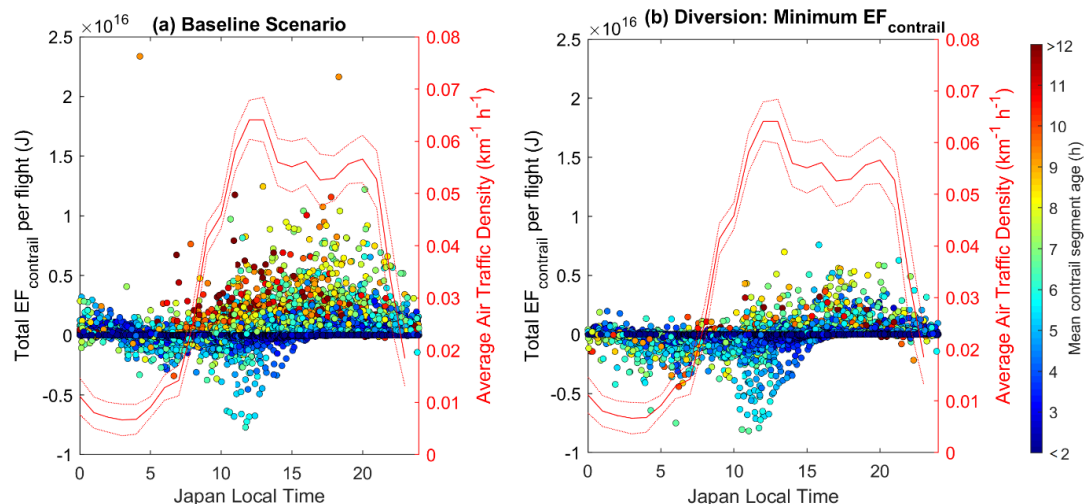


**Figure 2.** The  $EF_{\text{contrail}}$  for each flight vs. the time of day when these flights occur from one run of Monte Carlo simulation, where (a) is the baseline scenario; and (b) is the strategy with flight trajectories changed to achieve a minimum  $EF_{\text{contrail}}$ . All contrail-forming flights in the CARATS Open Data are included, and the mean contrail segment age is shown by the symbol colour. The red lines refer to the right-axis, showing the air traffic density  $> 20,000$  feet (mean  $\pm 1.96\sigma$ ) vs. the time of the day.

### 3.1.4. Minimum $EF_{\text{contrail}}$ with No Fuel Penalty

In this strategy, we explore the same objective function of a minimum  $EF_{\text{contrail}}$ , but with an added constraint of diverting flights only when they do not incur a fuel penalty. This is possible if the alternative trajectory has a more favourable wind condition, or is closer to the optimal cruising altitude (for specific aircraft types and mass). For this strategy, 7.63% [7.47, 7.81%] of all flights are diverted to reduce both the  $EF_{\text{contrail}}$  and TFC by 52.1% [42.5, 60.8%] and 0.86% [0.84, 0.88%]. We note that the number of flights diverted and the mitigated  $EF_{\text{contrail}}$  is approximately 50% less than in the minimum  $EF_{\text{contrail}}$  strategy with no constraints. Given the long-lived nature of  $CO_2$  emissions [68] together with large uncertainties in the  $EF_{\text{contrail}}$  from individual flights [28], and in the contrail climate impact (in terms of the global surface temperature response) [67,79], this constraint ensures, within the limits of the aircraft fuel consumption model, that the diversion of specific flights does not lead to unintended consequences of increasing total climate forcing. Contrary to perception, mitigating the contrail effects of aviation does not require an increase in fuel consumption.

### 3.1.5. Minimum $EF_{\text{total}}$

The strategy to minimise  $EF_{\text{total}}$  ( $EF_{\text{contrail}}$  and  $EF_{CO_2}$ ) reduces  $EF_{\text{contrail}}$  by the same magnitude as the minimum  $EF_{\text{contrail}}$  strategy with no constraints (105% [91.8, 125%]) and in addition achieves a small reduction in the TFC (0.40% [0.31, 0.47%]). The reduction in  $EF_{\text{total}}$  (66.8% [57.4, 83.9%]) is not much larger than that achieved in the minimum  $EF_{\text{contrail}}$  strategy with no constraints (66.7% [57.2, 83.7%]). However, this small gain of 0.1% is achieved at the cost of diverting significantly more flights (20.1% [19.9, 20.3%] vs. 15.3% [15.0, 15.7%]). This is because reductions in  $EF_{\text{total}}$  are almost entirely composed of reductions in the  $EF_{\text{contrail}}$ . Reductions in  $EF_{\text{total}}$  from fuel savings are very small despite the long atmospheric lifetime of  $CO_2$  [68]. A sensitivity analysis utilising a 1000-year TH for the  $CO_2$  AGWP TH, which gives greater weight to  $CO_2$ , yielded similar results. For these reasons, we do not consider the minimum  $EF_{\text{total}}$  strategy when evaluating the impact of different flight diversion strategies to ATM in Section 3.2.

## 3.2. Loss of Separation

Current ATM systems could present a barrier to implementing a targeted contrail diversion strategy at scale. Flight altitude changes as a result of contrail diversions are analogous to cases where flights are diverted due to bad weather and severe turbulence [80,81]. Such diversions reduce airspace capacity, increase airspace complexity and the workload of air traffic controllers because flights have to be tactically managed to maintain a safe separation distance.

In this subsection, we evaluate the feasibility of implementing the three most promising contrail diversion strategies on the perspective of ATM: (i) the small-scale diversion strategy that was proposed by Teoh et al. [28], showing that a diversion of up to 1.7% of all flights (with the largest  $EF_{\text{contrail}}$ ) leads to a reduction in total  $EF_{\text{contrail}}$  by 59.3% [52.4, 65.6%]; (ii) the minimum  $EF_{\text{contrail}}$  strategy, where diverting 15.3% [15.0, 15.7%] of all flights achieves a reduction of 105% ([91.8, 125%]) in the total  $EF_{\text{contrail}}$  (Section 3.1.3); and (iii) the same minimum  $EF_{\text{contrail}}$  strategy, but with an added fuel penalty constraint where 7.63% [7.47, 7.81%] of all flights are diverted to reduce the total  $EF_{\text{contrail}}$  by 52.1% [42.5, 60.8%] (Section 3.1.4).

For these three diversion strategies, Table 2 provides a summary of the total number of flights diverted and the number of incidences where flights experience a LOS, while Figure 3 shows the hourly variation of these quantities for the 42 days of air traffic data available. There is a day-to-day variation in the number of flights diverted that depends on ambient meteorological conditions [28], and ATM conflicts generally occur between 09:00 and 23:00 local time (Figure 3). Although the total number of flights diverted in the minimum  $EF_{\text{contrail}}$  strategy (with no constraints) is approximately 10 times higher than the small-scale diversion strategy (22,696 vs. 2196 flights), there is a lower proportion of flights in conflict relative to the total number of flights diverted (9.06% vs. 13.8%).

This is because the small-scale diversion strategy primarily diverts flights between 15:00 and 22:00 local time (Figure 3a, left), when ATD is high (as shown in Figure 2) and when ATM conflicts occur more frequently (Figure 3a, right). Conversely, the minimum  $EF_{\text{contrail}}$  strategy (with no constraints) also diverts flights before 09:00 local time (Figure 3b, left), when ATD is low (Figure 2) so that these diversions introduce few ATM conflicts (Figure 3b, right). The number of ATM impacts in the third strategy (minimum  $EF_{\text{contrail}}$  with fuel penalty constraints) lies in between those of the small-scale diversion strategy and the unconstrained minimum  $EF_{\text{contrail}}$  strategy (Table 2 and Figure 3c).

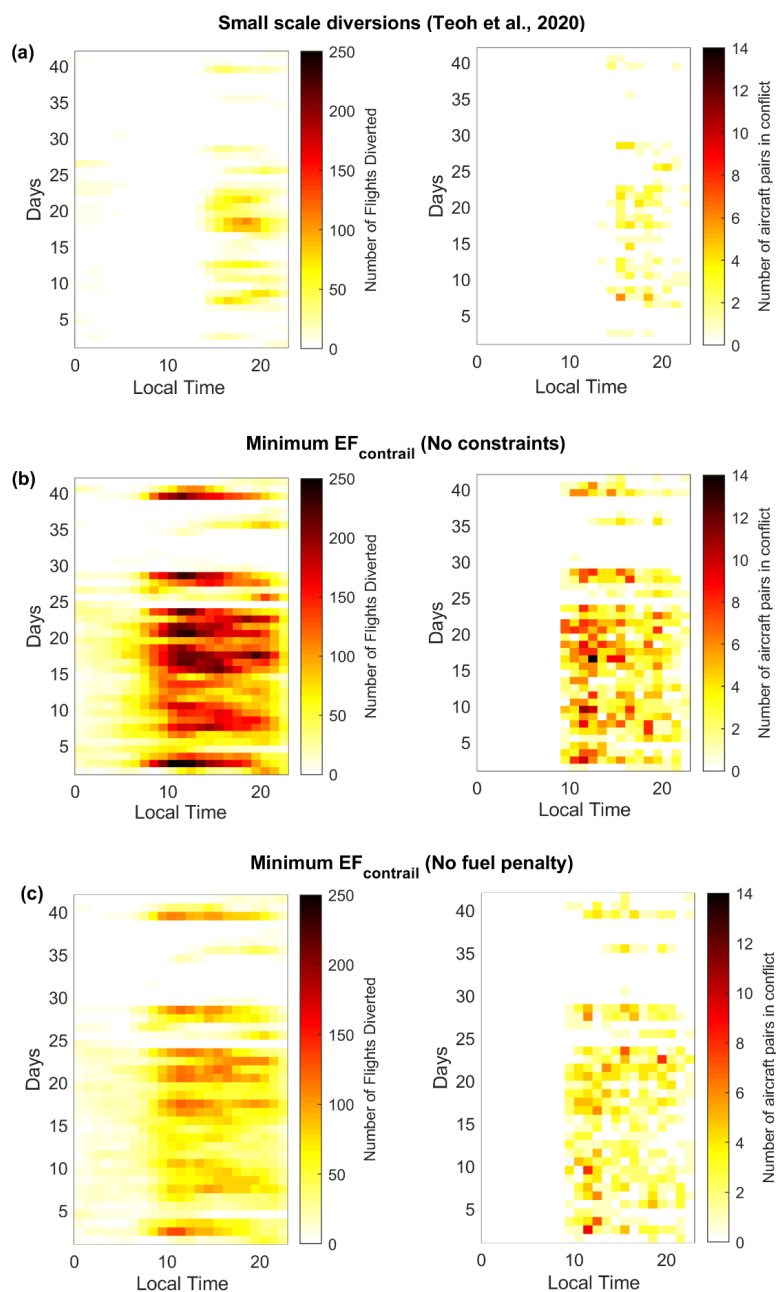


**Figure 3.** Daily variations in the number of flights diverted (left) and ATM conflicts (right) at different times of the day for: (a) the small-scale diversion strategy proposed by Teoh et al. [28]; (b) the minimum  $EF_{\text{contrail}}$  strategy with no constraints (Section 3.1.3); and (c) the minimum  $EF_{\text{contrail}}$  strategy with fuel penalty constraints (Section 3.1.4). The CARATS Open Data consists of 42 days of air traffic data, and each row represents the results for one day.

**Table 2.** Total number (and percentage) of flights diverted, and summary statistics of the resulting air traffic management (ATM) conflicts for: (i) the small-scale diversion proposed by Teoh et al. [28]; the minimum  $EF_{\text{contrail}}$  strategy with (ii) no constraints (Section 3.1.3); and (iii) with constraints where only flights that do not incur a fuel penalty are diverted (Section 3.1.4).

Strategy	Total (and %) of Flights Diverted	Total No. of Aircraft Pairs in Conflict	Total No. of Flights in Conflict	Ratio of Flights in Conflict to the Total No. of Flights Diverted (%)
Small-scale diversions [28]	2196 (1.47%)	169	304	13.8%
Min $EF_{\text{contrail}}$	22696 (15.2%)	1181	2056	9.06%
Min $EF_{\text{contrail}}$ (no fuel penalty)	11386 (7.63%)	678	1222	10.7%

These results demonstrate that flexibility may exist in the current ATM system to implement a contrail diversion strategy: although there could be constraints in diverting flights with the largest  $EF_{\text{contrail}}$  at times of high ATD, the diversion of flights to form cooling contrails before dawn does not introduce ATM complications and could be exploited to mitigate the contrail climate forcing.

#### 4. Conclusions

Contrails forming behind aircraft can persist and transform into contrail cirrus clouds, spreading across large areas of the sky. Although contrails have short lifetimes of up to a day, their climate forcing could reach a magnitude that is comparable to aviation's cumulative  $\text{CO}_2$  emissions from past traffic. Several mitigation solutions have been proposed to mitigate the contrail climate forcing, including the use of cleaner-burning engines, alternative fuels, and different forms of flight diversion strategies. However, the widespread use of cleaner-burning engines and alternative fuels will take decades, leaving flight diversion strategies as a feasible option that could be implemented in the near-term.

In this paper, we evaluate the efficacy of mitigating the contrail climate forcing with different vertical flight diversion strategies. For flights in the Japanese airspace, alternative trajectories are generated for each flight by modifying the aircraft cruising altitude by  $\pm 2000$  feet. Contrails that are produced for these sets of trajectories are then simulated using the CoCiP contrail model. To evaluate the effectiveness of different strategies, trajectories are selected to minimise one of the following objective functions: (i) initial contrail length; (ii) contrail  $RF'$ ; (iii)  $EF_{\text{contrail}}$ ; (iv)  $EF_{\text{contrail}}$ , subjected to constraints where diverted flights do not incur a fuel penalty; and (v)  $EF_{\text{total}}$  that accounts for the EF of both contrails and  $\text{CO}_2$ .

Depending on the choice of strategy, different efficacies in mitigating the contrail climate forcing are found. Contrail avoidance can lead to a suboptimal outcome in mitigating the contrail climate forcing by  $EF_{\text{contrail}}$  because it avoids not only strongly warming contrails, but also short-lived contrails with negligible radiative significance and avoids contrails that cool during the day. Similarly, a strategy minimising the contrail  $RF'$  could favour the formation of long-lived contrails, which can have a large  $EF_{\text{contrail}}$  when a small  $RF'$  is integrated over a long lifetime. Contrail mitigation appears to be most effective by minimising the climate forcing that is accumulated over a contrail's lifetime: for the study area considered, a diversion of 15.3% [15.0, 15.7%] of all flights minimising the formation of long-lived contrails and forming cooling contrails can reduce the aggregated  $EF_{\text{contrail}}$  and  $EF_{\text{total}}$  by 105% [91.8, 125%] and 66.7% [57.2, 83.7%], respectively, but with a 0.70% [0.66, 0.73%] increase in TFC. The same strategy (minimum  $EF_{\text{contrail}}$ ) with an added constraint of diverting flights only when they do not incur a fuel penalty, diverts 7.63% [7.47, 7.81%] of flights, reduces the  $EF_{\text{contrail}}$  by 52.1% [42.5, 60.8%] and simultaneously reduces TFC by 0.86% [0.84, 0.88%]. Finally, a strategy minimising the  $EF_{\text{total}}$  showed diminishing returns: the TFC is reduced by 0.40% [0.31, 0.47%], but this necessitates the diversion of 20.1% [19.9, 20.3%] of all flights and the further reduction in  $EF_{\text{total}}$  is negligible when compared with the minimum  $EF_{\text{contrail}}$  strategy with no constraints.

We then evaluate the impacts to ATM from three flight diversion strategies, in particular: (i) the small-scale diversion from Teoh et al. [28]; and the minimum  $EF_{\text{contrail}}$  strategy (ii) without constraints; and (iii) with a constraint on fuel penalty. For all three strategies, the proportion of flights in conflict relative to the number of flights diverted is below 15%. The large majority of ATM conflicts occur when the ATD is high (between 09:00 and 23:00 local time), but flights that are rerouted to produce cooling contrails at times of low ATD (before 09:00 local time) do not cause ATM conflicts. These results suggest that some form of flight diversion strategy could be implemented under the current ATM system without the need for new communication, navigation and surveillance (CNS) ATM technologies, such as considered in the US Federal Aviation Administration's Next Generation Air Transport System (NextGen) and the European Commission's Single European Sky (SES) initiative [82,83].

As contrails are short-lived relative to  $CO_2$  emissions, which can remain in the atmosphere for more than a millennium, an implementation of a vertical flight diversion strategy could significantly reduce the warming effect of aviation at short time scales. This presents the aviation industry with an opportunity to rapidly and significantly reduce its overall contribution to global warming.

**Author Contributions:** Conceptualization, methodology and investigation, R.T., U.S., and M.E.J.S.; software, R.T., U.S.; writing, review and editing, R.T., U.S. and M.E.J.S.; visualisation, R.T., M.E.J.S. All authors have read and agreed to the published version of the manuscript.

**Funding:** This research received no external funding.

**Acknowledgments:** The CARATS Open Data was supplied by the Electronic Navigation Research Institute (ENRI). R. Teoh received funding from The Lloyds Register Foundation, and the Skempton Scholarship from the Department of Civil and Environmental Engineering, Imperial College London.

**Conflicts of Interest:** The authors declare no conflict of interest.

## References

1. Kärcher, B.; Kleine, J.; Sauer, D.; Voigt, C. Contrail formation: Analysis of sublimation mechanisms. *Geophys. Res. Lett.* **2018**, *45*, 13547–13552. [[CrossRef](#)]
2. Schumann, U. Formation, properties and climatic effects of contrails. *Comptes Rendus Phys.* **2005**, *6*, 549–565. [[CrossRef](#)]
3. Schumann, U. On conditions for contrail formation from aircraft exhausts. *Meteorol. Z.* **1996**, *5*, 4–23. [[CrossRef](#)]
4. Kärcher, B.; Yu, F. Role of aircraft soot emissions in contrail formation. *Geophys. Res. Lett.* **2009**, *36*. [[CrossRef](#)]
5. Schumann, U. A contrail cirrus prediction model. *Geosci. Model Dev.* **2012**, *5*, 543–580. [[CrossRef](#)]
6. Kärcher, B. The importance of contrail ice formation for mitigating the climate impact of aviation. *J. Geophys. Res. Atmos.* **2016**, *121*, 3497–3505. [[CrossRef](#)]
7. Jensen, E.; Toon, O.B.; Kinne, S.; Sachse, G.W.; Anderson, B.E.; Chan, K.R.; Twohy, C.H.; Gandrud, B.; Heymsfield, A.; Miake-Lye, R.C. Environmental conditions required for contrail formation and persistence. *J. Geophys. Res. Space Phys.* **1998**, *103*, 3929–3936. [[CrossRef](#)]
8. Kärcher, B. Formation and radiative forcing of contrail cirrus. *Nat. Commun.* **2018**, *9*, 1824. [[CrossRef](#)] [[PubMed](#)]
9. Vazquez-Navarro, M.; Mannstein, H.; Kox, S. Contrail life cycle and properties from 1 year of MSG/SEVIRI rapid-scan images. *Atmos. Chem. Phys.* **2015**, *15*, 8739–8749. [[CrossRef](#)]
10. Schumann, U.; Graf, K.; Mannstein, H.; Mayer, B. Contrails: Visible aviation induced climate impact. In *Atmospheric Physics*; Springer: Berlin/Heidelberg, Germany, 2012; pp. 239–257. [[CrossRef](#)]
11. Irvine, E.; Hoskins, B.J.; Shine, K.P. A simple framework for assessing the trade-off between the climate impact of aviation carbon dioxide emissions and contrails for a single flight. *Environ. Res. Lett.* **2014**, *9*, 064021. [[CrossRef](#)]
12. Burkhardt, U.; Kärcher, B. Global radiative forcing from contrail cirrus. *Nat. Clim. Chang.* **2011**, *1*, 54–58. [[CrossRef](#)]
13. Mannstein, H.; Schumann, U. Aircraft induced contrail cirrus over Europe. *Meteorol. Z.* **2005**, *14*, 549–554. [[CrossRef](#)]

14. Duda, D.P.; Minnis, P.; Nguyen, L. Estimates of cloud radiative forcing in contrail clusters using GOES imagery. *J. Geophys. Res. Space Phys.* **2001**, *106*, 4927–4937. [[CrossRef](#)]
15. Schumann, U.; Mayer, B.; Graf, K.; Mannstein, H. A parametric radiative forcing model for contrail cirrus. *J. Appl. Meteorol. Clim.* **2012**, *51*, 1391–1406. [[CrossRef](#)]
16. Fuglestedt, J.S.; Shine, K.P.; Berntsen, T.; Cook, J.; Lee, D.; Stenke, A.; Skeie, R.; Velders, G.J.M.; Waitz, I. Transport impacts on atmosphere and climate: Metrics. *Atmos. Environ.* **2010**, *44*, 4648–4677. [[CrossRef](#)]
17. Meerkötter, R.; Schumann, U.; Doelling, D.R.; Minnis, P.; Nakajima, T.; Tsushima, Y. Radiative forcing by contrails. *Ann. Geophys.* **1999**, *17*, 1080–1094. [[CrossRef](#)]
18. Schumann, U.; Graf, K. Aviation-induced cirrus and radiation changes at diurnal timescales. *J. Geophys. Res. Atmos.* **2013**, *118*, 2404–2421. [[CrossRef](#)]
19. Newinger, C.; Burkhardt, U. Sensitivity of contrail cirrus radiative forcing to air traffic scheduling. *J. Geophys. Res. Space Phys.* **2012**, *117*, D10205. [[CrossRef](#)]
20. Bock, L.; Burkhardt, U. The temporal evolution of a long-lived contrail cirrus cluster: Simulations with a global climate model. *J. Geophys. Res. Atmos.* **2016**, *121*, 3548–3565. [[CrossRef](#)]
21. Schumann, U.; Penner, J.E.; Chen, Y.; Zhou, C.; Graf, K. Dehydration effects from contrails in a coupled contrail–climate model. *Atmos. Chem. Phys.* **2015**, *15*, 11179–11199. [[CrossRef](#)]
22. Lee, D.; Pitari, G.; Grewe, V.; Gierens, K.; Penner, J.; Petzold, A.; Prather, M.; Schumann, U.; Bais, A.; Berntsen, T.; et al. Transport impacts on atmosphere and climate: Aviation. *Atmos. Environ.* **2010**, *44*, 4678–4734. [[CrossRef](#)] [[PubMed](#)]
23. Schumann, U.; Graf, K.; Mannstein, H. Potential to reduce the climate impact of aviation by flight level changes. *AIAA paper* **2011**, *3376*, 1–22. [[CrossRef](#)]
24. Chen, C.-C.; Gettelman, A. Simulated radiative forcing from contrails and contrail cirrus. *Atmos. Chem. Phys.* **2013**, *13*, 12525–12536. [[CrossRef](#)]
25. Yi, B.; Yang, P.; Liou, K.-N.; Minnis, P.; Penner, J.E. Simulation of the global contrail radiative forcing: A sensitivity analysis. *Geophys. Res. Lett.* **2012**, *39*. [[CrossRef](#)]
26. Minnis, P.; Palikonda, R.; Walter, B.J.; Ayers, J.K.; Mannstein, H. Contrail properties over the eastern North Pacific from AVHRR data. *Meteorol. Z.* **2005**, *14*, 515–523. [[CrossRef](#)]
27. Schumann, U.; Heymsfield, A.J. On the life cycle of individual contrails and contrail cirrus. *Meteorol. Monogr.* **2017**, *58*, 3.1–3.24. [[CrossRef](#)]
28. Teoh, R.; Schumann, U.; Majumdar, A.; Stettler, M.E. Mitigating the climate forcing of aircraft contrails by small-scale diversions and technology adoption. *Environ. Sci. Technol.* **2020**, *54*, 2941–2950. [[CrossRef](#)]
29. Boies, A.M.; Stettler, M.E.J.; Swanson, J.J.; Johnson, T.J.; Olfert, J.; Johnson, M.; Eggersdorfer, M.L.; Rindlisbacher, T.; Wang, J.; Thomson, K.; et al. Particle emission characteristics of a gas turbine with a double annular combustor. *Aerosol Sci. Technol.* **2015**, *49*, 842–855. [[CrossRef](#)]
30. Stickles, R.; Barrett, J. *TAPS II Combustor Final Report. CLEEN Program; Federal Aviation Administration (FAA): Washington, DC, USA, 2013.*
31. Lobo, P.; Durdina, L.; Smallwood, G.J.; Rindlisbacher, T.; Siegerist, F.; Black, E.A.; Yu, Z.; Mensah, A.A.; Hagen, D.E.; Miake-Lye, R.C.; et al. Measurement of aircraft engine non-volatile pm emissions: Results of the aviation-particle regulatory instrumentation demonstration experiment (A-PRIDE) 4 campaign. *Aerosol Sci. Technol.* **2015**, *49*, 472–484. [[CrossRef](#)]
32. Moore, R.; Thornhill, K.L.; Weinzierl, B.; Sauer, D.; D’Ascoli, E.; Kim, J.; Lichtenstern, M.; Scheibe, M.; Beaton, B.; Beyersdorf, A.J.; et al. Biofuel blending reduces particle emissions from aircraft engines at cruise conditions. *Nature* **2017**, *543*, 411–415. [[CrossRef](#)]
33. Twomey, S. Pollution and the planetary albedo. *Atmos. Environ. (1967)* **1974**, *8*, 1251–1256. [[CrossRef](#)]
34. Howe, S.; Kolios, A.; Brennan, F.P. Environmental life cycle assessment of commercial passenger jet airliners. *Transp. Res. Part D Transp. Environ.* **2013**, *19*, 34–41. [[CrossRef](#)]
35. Dray, L.; Evans, A.; Reynolds, T.; Schäfer, A.W.; Vera-Morales, M.; Bosbach, W. Airline fleet replacement funded by a carbon tax: An integrated assessment. *Transp. Policy* **2014**, *34*, 75–84. [[CrossRef](#)]
36. Chereau, D.; Kleffmann, K.; Callan, P. Dossier: Fuel for Thought | Airlines. Available online: <https://airlines.iata.org/analysis/dossier-fuel-for-thought> (accessed on 20 December 2019).
37. Schäfer, A.W.; Waitz, I.A. Air transportation and the environment. *Transp. Policy* **2014**, *34*, 1–4. [[CrossRef](#)]
38. Bock, L.; Burkhardt, U. Contrail cirrus radiative forcing for future air traffic. *Atmos. Chem. Phys.* **2019**, *19*, 8163–8174. [[CrossRef](#)]

39. Caiazzo, F.; Agarwal, A.; Speth, R.L.; Barrett, S.R. Impact of biofuels on contrail warming. *Environ. Res. Lett.* **2017**, *12*, 114013. [[CrossRef](#)]
40. Gierens, K.; Spichtinger, P. On the size distribution of ice-supersaturated regions in the upper troposphere and lowermost stratosphere. *Ann. Geophys.* **2000**, *18*, 499–504. [[CrossRef](#)]
41. Spichtinger, P.; Gierens, K.; Leiterer, U.; Dier, H. Ice supersaturation in the tropopause region over Lindenberg, Germany. *Meteorol. Z.* **2003**, *12*, 143–156. [[CrossRef](#)]
42. Dickson, N.C.; Gierens, K.M.; Rogers, H.L.; Jones, R.L. Probabilistic description of ice-supersaturated layers in low resolution profiles of relative humidity. *Atmos. Chem. Phys.* **2010**, *10*, 6749–6763. [[CrossRef](#)]
43. Lim, Y.; Gardi, A.G.M.; Sabatini, R. Optimal aircraft trajectories to minimize the radiative impact of contrails and CO<sub>2</sub>. *Energy Procedia* **2017**, *110*, 446–452. [[CrossRef](#)]
44. Mannstein, H.; Spichtinger, P.; Gierens, K. A note on how to avoid contrail cirrus. *Transp. Res. Part D Transp. Environ.* **2005**, *10*, 421–426. [[CrossRef](#)]
45. Williams, V.; Noland, R.B. Variability of contrail formation conditions and the implications for policies to reduce the climate impacts of aviation. *Transp. Res. Part D Transp. Environ.* **2005**, *10*, 269–280. [[CrossRef](#)]
46. Avila, D.; Sherry, L.; Thompson, T. Reducing global warming by airline contrail avoidance: A case study of annual benefits for the contiguous United States. *Transp. Res. Interdiscip. Perspect.* **2019**, *2*, 100033. [[CrossRef](#)]
47. Yin, F.; Grewe, V.; Frömming, C.; Yamashita, H. Impact on flight trajectory characteristics when avoiding the formation of persistent contrails for transatlantic flights. *Transp. Res. Part D Transp. Environ.* **2018**, *65*, 466–484. [[CrossRef](#)]
48. Grewe, V.; Matthes, S.; Frömming, C.; Brinkop, S.; Jöckel, P.; Gierens, K.; Champougny, T.; Fuglestedt, J.; Haslerud, A.; Irvine, E.; et al. Feasibility of climate-optimized air traffic routing for trans-Atlantic flights. *Environ. Res. Lett.* **2017**, *12*, 034003. [[CrossRef](#)]
49. Rosenow, J.; Fricke, H.; Luchkova, T.; Schultz, M. Minimizing contrail formation by rerouting around dynamic ice-supersaturated regions. *Aeronaut. Aerosp. Open Access J.* **2018**, *2*, 1. [[CrossRef](#)]
50. Filippone, A. Assessment of aircraft contrail avoidance strategies. *J. Aircr.* **2015**, *52*, 872–877. [[CrossRef](#)]
51. Matthes, S.; Schumann, U.; Grewe, V.; Frömming, C.; Dahlmann, K.; Koch, A.; Mannstein, H. *Climate Optimized Air Transport*; Springer: Berlin/Heidelberg, Germany, 2012; pp. 727–746. [[CrossRef](#)]
52. Myhre, G.; Stordal, F. On the tradeoff of the solar and thermal infrared radiative impact of contrails. *Geophys. Res. Lett.* **2001**, *28*, 3119–3122. [[CrossRef](#)]
53. Stuber, N.; Forster, P.M.; Rädel, G.; Shine, K.P. The importance of the diurnal and annual cycle of air traffic for contrail radiative forcing. *Nature* **2006**, *441*, 864–867. [[CrossRef](#)]
54. Stettler, M.E.; Eastham, S.; Barrett, S.R. Air quality and public health impacts of UK airports. Part I: Emissions. *Atmos. Environ.* **2011**, *45*, 5415–5424. [[CrossRef](#)]
55. Nuic, A. *User Manual for the Base of Aircraft Data (BADA) Revision 3.12.*; Eurocontrol Experimental Centre: Les Bordes, France, 2014; Volume EEC.
56. Schumann, U. Influence of propulsion efficiency on contrail formation. *Aerosp. Sci. Technol.* **2000**, *4*, 391–401. [[CrossRef](#)]
57. Teoh, R.; Stettler, M.E.; Majumdar, A.; Schumann, U.; Graves, B.; Boies, A.M. A methodology to relate black carbon particle number and mass emissions. *J. Aerosol Sci.* **2019**, *132*, 44–59. [[CrossRef](#)]
58. Jeßberger, P.; Voigt, C.; Schumann, U.; Sölch, I.; Schlager, H.; Kaufmann, S.; Petzold, A.; Schäuble, D.; Gayet, J.-F. Aircraft type influence on contrail properties. *Atmos. Chem. Phys.* **2013**, *13*, 11965–11984. [[CrossRef](#)]
59. Schumann, U.; Jeßberger, P.; Voigt, C. Contrail ice particles in aircraft wakes and their climatic importance. *Geophys. Res. Lett.* **2013**, *40*, 2867–2872. [[CrossRef](#)]
60. Schumann, U.; Baumann, R.; Baumgardner, D.; Bedka, S.T.; Duda, D.P.; Freudenthaler, V.; Gayet, J.-F.; Heymsfield, A.J.; Minnis, P.; Quante, M.; et al. Properties of individual contrails: A compilation of observations and some comparisons. *Atmospheric Chem. Phys.* **2017**, *17*, 403–438. [[CrossRef](#)]
61. Voigt, C.; Schumann, U.; Jurkat, T.; Schäuble, D.; Schlager, H.; Petzold, A.; Gayet, J.-F.; Krämer, M.; Schneider, J.; Borrmann, S.; et al. In-situ observations of young contrails—Overview and selected results from the CONCERT campaign. *Atmos. Chem. Phys.* **2010**, *10*, 9039–9056. [[CrossRef](#)]
62. Hersbach, H.; Bell, B.; Berrisford, P.; Hirahara, S.; Horányi, A.; Muñoz-Sabater, J.; Nicolas, J.; Peubey, C.; Radu, R.; Schepers, D.; et al. The ERA5 global reanalysis. *Q. J. R. Meteorol. Soc.* **2020**, *146*, 1999–2049. [[CrossRef](#)]

63. ECMWF. Forecast User Guide—5.1 Generation of the Ensemble, Ensemble of Data Assimilations (EDA). Available online: <https://confluence.ecmwf.int/display/FUG/Ensemble+of+Data+Assimilations+-+EDA> (accessed on 7 August 2020).
64. Gounou, A.; Hogan, R.J. A sensitivity study of the effect of horizontal photon transport on the radiative forcing of contrails. *J. Atmos. Sci.* **2007**, *64*, 1706–1716. [[CrossRef](#)]
65. Forster, L.; Emde, C.; Mayer, B.; Unterstrasser, S. Effects of three-dimensional photon transport on the radiative forcing of realistic contrails. *J. Atmos. Sci.* **2012**, *69*, 2243–2255. [[CrossRef](#)]
66. Rosenow, J.; Fricke, H. Individual condensation trails in aircraft trajectory optimization. *Sustainability* **2019**, *11*, 6082. [[CrossRef](#)]
67. Bickel, M.; Ponater, M.; Bock, L.; Burkhardt, U.; Reineke, S. Estimating the effective radiative forcing of contrail cirrus. *J. Clim.* **2020**, *33*, 1991–2005. [[CrossRef](#)]
68. Joos, F.; Roth, R.; Fuglestad, J.S.; Peters, G.G.; Enting, I.G.; Von Bloh, W.; Brovkin, V.; Burke, E.J.; Eby, M.; Edwards, N.R.; et al. Carbon dioxide and climate impulse response functions for the computation of greenhouse gas metrics: A multi-model analysis. *Atmos. Chem. Phys.* **2013**, *13*, 2793–2825. [[CrossRef](#)]
69. Wilkerson, J.; Jacobson, M.Z.; Malwitz, A.; Balasubramanian, S.; Wayson, R.; Fleming, G.; Naiman, A.D.; Lele, S.K. Analysis of emission data from global commercial aviation: 2004 and 2006. *Atmos. Chem. Phys.* **2010**, *10*, 6391–6408. [[CrossRef](#)]
70. NASA. By the Numbers | Earth—NASA Solar System Exploration. Available online: <https://solarsystem.nasa.gov/planets/earth/by-the-numbers/> (accessed on 27 November 2019).
71. Nuic, A.; Poles, D.; Mouillet, V. BADA: An advanced aircraft performance model for present and future ATM systems. *Int. J. Adapt. Control. Signal Process.* **2010**, *24*, 850–866. [[CrossRef](#)]
72. Poll, D.; Schumann, U. An estimation method for the fuel burn and other performance characteristics of civil transport aircraft in the cruise. Part 1 fundamental quantities and governing relations for a general atmosphere. *Aeronaut. J.* **2020**, 1–39. [[CrossRef](#)]
73. Eurocontrol. BADA, ATM’s Most Comprehensive Aircraft Performance Model, Just Got Even Better | EUROCONTROL. Available online: <https://www.eurocontrol.int/news/bada-atms-most-comprehensive-aircraft-performance-model-just-got-even-better> (accessed on 27 July 2020).
74. Tobaruela, G.; Schuster, W.; Majumdar, A.; Ochieng, W.Y.; Martínez, L.; Hendrickx, P. A method to estimate air traffic controller mental workload based on traffic clearances. *J. Air Transp. Manag.* **2014**, *39*, 59–71. [[CrossRef](#)]
75. ICAO. *Air Traffic Management—Procedures for Air Navigation Services*, 16th ed.; International Civil Aviation Organisation: Montreal, QC, Canada, 2016; Volume Doc 4444.
76. Tobaruela, G. *A Framework to Assess the Ability of Automation to Deliver Capacity Targets in European Airspace*; Center for Transport Studies; Imperial College London: London, UK, 2015.
77. Graf, K.; Schumann, U.; Mannstein, H.; Mayer, B. Aviation induced diurnal North Atlantic cirrus cover cycle. *Geophys. Res. Lett.* **2012**, *39*. [[CrossRef](#)]
78. Haywood, J.; Allan, R.P.; Bornemann, J.; Forster, P.M.; Francis, P.N.; Milton, S.; Rädcl, G.; Rap, A.; Shine, K.P.; Thorpe, R. A case study of the radiative forcing of persistent contrails evolving into contrail-induced cirrus. *J. Geophys. Res. Space Phys.* **2009**, *114*, 114. [[CrossRef](#)]
79. Schumann, U.; Mayer, B. Sensitivity of surface temperature to radiative forcing by contrail cirrus in a radiative-mixing model. *Atmos. Chem. Phys.* **2017**, *17*, 13833–13848. [[CrossRef](#)]
80. Klein, A.; Kavoussi, S.; Lee, R.S. Weather Forecast Accuracy: Study of Impact on Airport Capacity and Estimation of Avoidable Costs. In Proceedings of the Eighth USA/Europe Air Traffic Management Research and Development Seminar, Napa, CA, USA, 29 June–2 July 2009.
81. Krozel, J.; Mitchell, J.; Polishchuk, V.; Prete, J. Capacity Estimation for Airspaces with Convective Weather Constraints. In *Guidance, Navigation, and Control Conference*; American Institute of Aeronautics and Astronautics (AIAA): Reston, VA, USA, 2007; p. 6451.
82. Federal Aviation Administration. Modernization of U.S. Airspace. Available online: <https://www.faa.gov/nextgen/> (accessed on 7 August 2020).
83. SESAR. Delivering the Single European Sky—Environmental Benefits. Available online: <http://www.sesarju.eu/node/718> (accessed on 7 August 2020).



© 2020 by the authors. Licensee MDPI, Basel, Switzerland. This article is an open access article distributed under the terms and conditions of the Creative Commons Attribution (CC BY) license (<http://creativecommons.org/licenses/by/4.0/>).